Recent Insights into Boron-Oxygen Related Degradation: Evidence of a Single Defect

Brett Hallam[1], Moonyong Kim[1], Malcolm Abbott[1], Nitin Nampalli[1], Tine Nærland[2], Bruno Stefani[1,3], Stuart Wenham[1]
[1] School of Photovoltaic and Renewable Energy Engineering, University of New South Wales, Sydney, NSW 2052, AUSTRALIA
[2] Institute for Energy Technology, Instituttveien 18, 2007 Kjeller, Norway (now with Ira A. Fulton Schools of Engineering, Arizona State University, Tempe, AZ 85287, USA)
[3] School of Engineering, Federal University of Rio Grande do Sul, Porto Alegre, BRAZIL

Abstract: Fast and slow boron-oxygen related degradation in p-type Czochralski silicon is often attributed to two separate defects due to the different time constants and the determination of different capture cross section ratios (*k*). However, recent work has suggested the possible involvement of a single defect [1],[2]. This study reviews recent evidence, and provides further evidence/analysis to demonstrate the involvement of a single defect, in four key areas: 1) Identical recombination properties in the fast and slow timescales [1]; 2) The ability to describe a multi-stage degradation of carrier lifetime with a single recombination active defect [1]; 3) The possible involvement of interstitial iron in accounting for higher apparent capture cross-section ratios during early stages of boron-oxygen related degradation and recombination with a high capture cross-section ratio remaining after permanent deactivation; 4) The ability to modulate the fraction of fast and slow degradation by thermal annealing without modulating the total extent of degradation or recombination properties [2]. A revised parameterisation of the B-O related recombination is also presented, which suggests a stronger influence of acceptor-level related recombination than has been previously reported.

Key words: Boron-oxygen, Czochralski silicon, light-induced degradation, carrier-induced degradation

1. Introduction

Boron-oxygen (B-O) related degradation has been studied for decades, with early identification of the degradation mechanism dating back to 1973 [3]. However, there is still significant debate over the structure, formation and passivation mechanisms for the defect [4]–[7]. One well-understood property of the degradation is that the presence of both oxygen and boron in Czochralski (Cz) silicon can cause a reduction of minority carrier lifetime in the presence of carrier injection [3],[8]. Full degradation of the minority carrier lifetime can take approximately 48 hours at room temperature. On finished PERC solar cells, this can cause a reduction in efficiency of 1.8% absolute, representing a performance degradation that can approach 10% relative [3],[9].

A well-known characteristic of B-O related degradation is that it occurs in two stages [10]. This degradation consists of a fast but slight decay of minority carrier lifetime with a time constant in the vicinity of 100 seconds, followed by a substantially slower and much more significant reduction of carrier lifetime with a time constant on the order of tens of hours [10]–[14]. For studies investigating the extent of fast and slow degradation, a linear dependence on the boron doping concentration was observed [11],[15].

Another well-known characteristic related to B-O defects is that on a pre-degraded sample, thermal annealing in the dark on can lead to a recovery of minority carrier lifetime, in a process called defect 'annihilation' [3],[9],[16]–[18]. However, this recovery is unstable, and exposure to subsequent carrier injection again results in a degradation of the minority carrier lifetime. The annihilation rate of B-O defects has been intensively investigated, although there is a significant spread in the values reported for the associated attempt frequency and activation energy [8],[10],[11],[19]–[23]. A condition known to result in the full recovery of minority carrier lifetime after B-O related degradation is an anneal at 200 °C for 10 minutes in the dark [24]. A large number of studies investigating B-O related degradation have used this condition [7],[11],[18],[20],[25]–[27]. Numerous other studies have used the same temperature for longer durations in the range of 20 minutes to 100 hours [13],[15],[28]–[34]. Other studies have used different temperatures in the range of 210 °C – 300 ° [35]–[38] and also 100 °C – 400 °C [39]. For the kinetics of the recovery process, one study observed a two-staged recovery of carrier lifetime for the fast decay and a single-staged recover for the slow decay [11], while another study reported that the lifetime recovery occurred in one stage for both the fast and slow decay [10]. However, none of the above studies investigated the influence of modulating

the dark annealing temperature on the fast and slow degradation behaviour.

In 2006, a study by Bothe *et al.* examined the recombination properties throughout B-O related degradation [11]. It was concluded that the fast and slow B-O related degradation was caused by two separate defects that form independently [11]. Often, these are called the fast-forming recombination centre (FRC) and the slow-forming recombination centre (SRC) [14],[40]. In addition to the differing time constants, one key argument presented for the existence of two separate defects was the determination of a different value for the ratio of the electron- (σ_n) and hole capture cross-section (σ_p) for the fast and slow B-O related degradation [11]. In early studies, the B-O defect was assumed to have a single defect level. Under this assumption, capture cross-section ratios (k) of approximately 100 and ten were determined for the fast- and slow decays, respectively [11]. However, there are significant variations in the k values reported in the literature for both the fast and slow degradation. For the slow degradation, early studies estimated k values of 5-10 [27],[37],[41]. More recent studies have estimated higher k values in the range of 10-12 [42], or 14 [43]. For the rapid degradation, a subsequent study presented values in the range of 65 – 86 [44], while a more recent paper by the same author estimated a value of 65 [43].

The variations of k values presented in the literature can at least be partially accounted for by the various assumptions and methods used in the respective papers. A numerical analysis of B-O defect recombination properties presented by Nampalli *et al.* highlighted that illuminated processes could also lead to small, yet statistically significant changes in the surface passivation throughout degradation that breaks the assumption of many methods used to analyse the B-O defect [45]. That paper highlighted that depending on the method used, median values in the range of 12-15 could be obtained.

Another source of error for the determined k values is the assumption of a single level defect for the B-O defect. An early study by Schmidt *et al.* observed that in some samples a shallow level defect was present in addition to a deep level defect [37]. That defect level was observed to decrease the lifetime at high carrier concentrations while having minimal effect at low carrier concentrations. More recent investigations have identified the existence of three defect charge states, and hence two separate defect levels for B-O related degradation in both the fast and slow timescales [44],[46]. While the donor level dominates recombination in low-injection, the presence of an acceptor level with a k value < 1 [46] causes a reduction of carrier lifetime predominately at higher injection levels. Therefore, taking the presence of an acceptor level into account will result in the determination of a larger k value for the donor level than that determined when assuming a single defect level.

With different k values and time constants for degradation, multiple subsequent theories have assumed that two separate defects are responsible for the fast and slow decay in carrier lifetime [40], [43],[44],[47],[48]. In a recent contribution, another argument was presented. It was suggested that processes to permanently deactivate the B-O complex only remove the combination activity of defects that form in the slow timescale, with recombination activity associated with degradation in the fast timescale, remaining [4].

However, there are also several arguments to suggest a single defect is responsible for both the fast and slow B-O related degradation. This paper aims to review the recent advancements in the understanding of B-O related degradation in silicon solar cells. It collates recent evidence to suggest the existence of a single B-O defect, along with providing more sophisticated modelling and new experimental evidence for the existence of a single B-O related defect. .The four key areas in support of this hypothesis are: 1) Identical recombination properties in the fast and slow timescales throughout degradation [1]. 2) Kinetic modelling demonstrating the ability to describe a multi-stage degradation of carrier lifetime [1]. 3) The possible involvement of interstitial iron in accounting for higher apparent k values during early stages of B-O related degradation and recombination with a high k value remaining after permanent deactivation. 4) The ability to modulate the fraction of fast and slow degradation without modulating the total extent of degradation or recombination properties [2].

Nomenclature

B-O	Boron-oxygen
DA	Dark Annealed
DG	Full Degradation
FRC	Fast-forming Recombination Centre
LS(t)	t seconds of Light Soaking
ODE	Ordinary Differential Equations
S1DP	Stage 1 Defect Precursor
S2DP	Stage 2 Defect Precursor
SRC	Slow Forming Recombination Centre
A1	State consisting of Stage 1 Defect Precursors
A2	State consisting of Stage 2 Defect Precursors
B	State of Formed Defect Complex
a	Acceptor Trap
E_t	Energy Level of the Trap
d	Donor Trap
f^0	Fractional Concentration of B-O Defects in the Neutral Charge
FDD	Fractional Defect Density
G	Generation Rate of Electron-Hole Pairs
J_0	Saturation Current Density
k	Capture Cross Section Ratio
κ	Reaction rate
Δn	Excess Charge Carrier Density
N	Normalized Concentration
NDD	Normalized Defect Density
σ_n	Electron Capture Cross Section
σ_p	Hole Capture Cross Section
τ	Charge Carrier Lifetime

τ_{ratio}	Ratio of lifetime in high and low injection
v	Characteristic Time Constant
W	Thickness of Wafer

2. Identical recombination properties of fast and slow B-O related degradation

While earlier studies have presented significant differences in the capture cross-section ratios for degradation in the fast and slow timescales, one striking similarity for recombination properties is the position of the donor and acceptor levels published in some papers (see Table 1). This data provides some evidence for the possibility of a single defect being responsible for B-O related degradation.

Table 1 Defect energy levels for the donor and acceptor levels of the B-O defect reported in the literature for fast and slow degradation.

	$E_{trap,d}$ (eV)	$E_{trap,a}$ (eV)	Ref.
Fast	E_C - (0.38±0.02)	E_V + (0.28±0.02)	[44]
	E_C - (0.34±0.02)	E_V + (0.31±0.02)	[49]
Slow	E_C - (0.41±0.03)		[41]
	E_C - (0.41±0.02)	E_V + (0.26±0.02)	[46]

Further evidence for the involvement of a single defect was present in our previous work [1]. This included a revised estimation of the ratio of capture cross-section of electrons to holes for the trap energy donor level ($E_{trap,d}$) of B-O related degradation in the fast timescale. In particular, we observed a substantially lower value of $\sigma_{n,d}/\sigma_{p,d}$ (19±4) [1] than that determined in earlier studies (in the range of 65 to 100) [11],[43],[44]. In addition, we demonstrated that identical recombination properties could be used to describe injection-level dependent lifetime curves throughout degradation in the fast and slow timescales [1]. A subsequent study by Niewelt *et al.* confirmed this much lower k value for the donor level of B-O related degradation in the fast timescale, obtaining a value of 18±1 [49]. It was observed that on some samples in the dataset, B-O related degradation could indeed be described by a single set of recombination properties throughout degradation. However, that was not true for all samples. It was concluded that the results could neither confirm nor refute the hypothesis that a single two-level defect is responsible for B-O related degradation. It should be noted that in [49], samples with the worst fit between the fully degraded lifetime curves and the presented parameterisation in the fast timescale (with the notation C1 and C2) also exhibited the worst fit after rapid degradation.

One limitation in our previous work was that the B-O related recombination properties were simulated in a simplified manner by using two separate defects with energy levels to represent the recombination activity associated with the donor and acceptor levels of the B-O defect [1]. Here, we present new modelling using two-level SRH recombination statistics for the experimental data presented in [1]. For this, symmetrical lifetime samples were fabricated on an example degradation curve was obtained from a 325 µm thick *p*-type Czochralski grown silicon wafer with a boron doping density of 3.6×10^{15} /cm^3. The wafer was RCA cleaned, and a 40 nm layer of amorphous silicon was deposited on both sides using plasma enhanced chemical vapor deposition (PECVD). Subsequently, the wafer was dark annealed at 200 °C for 15 minutes to annihilate all B-O defects. A degradation process was then performed at 303 ± 2 K using a halogen lamp with an illumination intensity of approximately 50 mW/cm^2. *In-situ* lifetime monitoring was performed throughout the degradation process using an automated quasi-steady-state photo-conductance [50] (QSS-PC) tool and the generalized analysis technique [51]. Further processing details can be found in [13].

The degradation curve of τ_{eff} as a function of the illumination duration is shown in Figure 1(a). It highlights the typical two-stage B-O related degradation that occurs under illumination. Red dashed lines in the graph indicate the times for which the inverse SRH lifetime ($1/\tau_{SRH}$) versus Δn curves are shown in Figure 1(b) throughout degradation. Specifically, curves are shown in the early, mid and late stages of fast degradation, as well as the mid and late stages of slow degradation.

For **Figure 1**(b), curve fitting was used to separate different bulk and surface lifetime components at each stage of degradation [52]. This included a saturation current density (J_0) of 7 ± 1 fA/cm^2 and a fixed injection-level independent bulk lifetime ($\tau_{bulk,0}$) of 14 ms. It should be noted that for the experimental data plotted in **Figure 1**(b), the $1/\tau_{SRH}$ curves were obtained by subtracting the inverse Auger ($1/\tau_{Aug}$), and the modelled dark saturation current density ($1/\tau_{J0}$) and injection-level independent bulk lifetime ($1/\tau_{bulk,0}$) components from the inverse effective minority carrier lifetime ($1/\tau_{eff}$) data. For the red modelled $1/\tau_{SRH}$ curves, a single set of recombination properties was used to describe B-O related degradation using a two-level SRH defect [53]. A trap energy donor level ($E_{trap,d}$) at 0.34 ± 0.01 eV below the conduction band (E_C) and trap energy acceptor level ($E_{trap,a}$) at 0.24 ± 0.01 eV above the valence band (E_V) were used to represent the 'negative U' properties of the B-O defect [4]. Capture cross-section ratios for electrons to holes for the donor and acceptor levels of $\sigma_{n,d}/\sigma_{p,d}$ = 18 and $\sigma_{n,a}/\sigma_{p,a}$ = 1/(60 ± 6) were used, respectively. A coupling capture cross-section ratio for electrons in the donor level to holes in the acceptor level of $\sigma_{n,d}/\sigma_{p,a}$ = 0.2 ± 0.04 was used. A summary of the B-O related recombination properties is shown in **Table 2**. For a comparison, the recent parameterization presented in [49] for rapid degradation is also shown.

Table 2 Parameterisation of the two-level SRH B-O defect determined in this work and Reference [49].

Parameter	This work	Reference [49]
$E_{trap,d}$ (eV)	E_C - (0.34 ± 0.01)	E_C - (0.34 ± 0.02)
$E_{trap,a}$ (eV)	E_V + (0.24 ± 0.01)	E_V + (0.31 ± 0.02)
$\sigma_{n,d}/\sigma_{p,d}$	18	18.1 ± 1
$\sigma_{n,a}/\sigma_{p,a}$	1/(60 ± 6)	1/(85.7 ± 1.5)
$\sigma_{n,d}/\sigma_{p,a}$	0.2 ± 0.04	1.2 ± 0.5

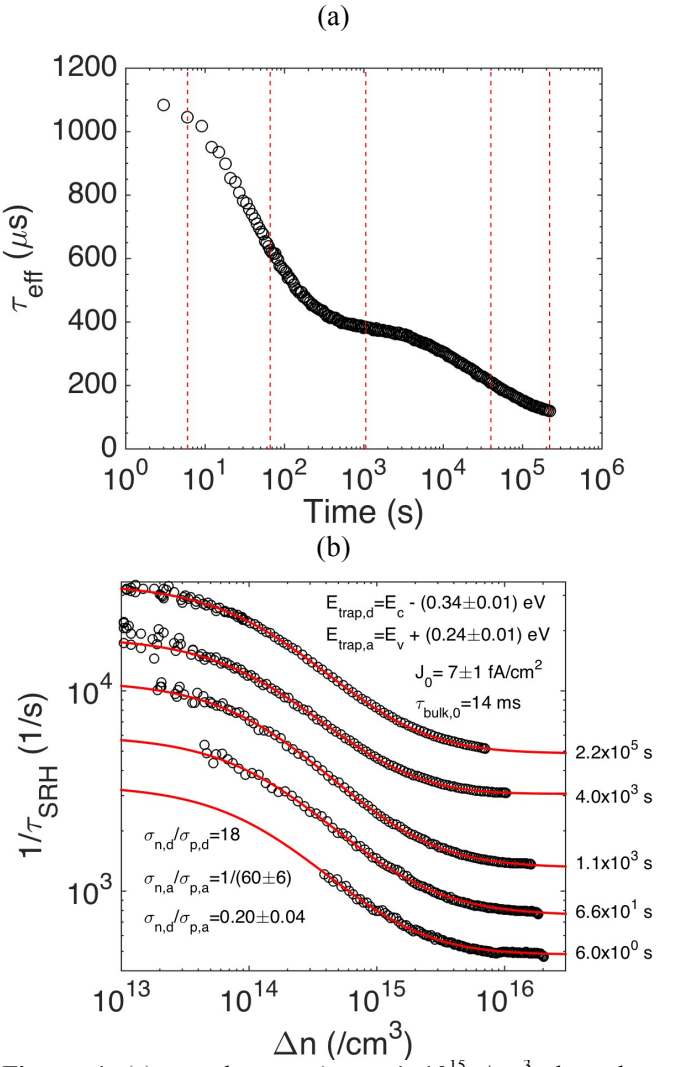

Figure 1 (a) τ_{eff} data at Δn = 1×10^{15} /cm^3 throughout degradation (303 K, 50 mW/cm^2 illumination). Red dashed lines indicate the times at which analysed curves are shown in (b). (b) Curves of inverse τ_{SRH} versus excess minority carrier density (Δn), after illumination of various durations indicated on the right-hand side of the graph (data from [1]). The inverse τ_{eff} data was corrected for Auger, J_0, and $\tau_{bulk,0}$ lifetime components ($1/\tau_{SRH} = 1/\tau_{eff} - 1/\tau_{Aug} - 1/\tau_{J0} - 1/\tau_{bulk,0}$).. Solid red lines show the modelled curves using a two-level SRH B-O defect assuming values shown in the graph.

As shown, an excellent agreement was achieved between the experimental data and the modelled curves, from all stages of degradation using the single set of recombination properties. For the fully degraded lifetime curve (after 2.2×10^5 s of illumination), the modelled SRH related inverse lifetime gave an excellent representation of the actual $1/\tau_{eff} - 1/\tau_{Aug}$ data. Furthermore, the modelled curve was insensitive to reasonable changes in J_0 (from 0 to 20 fA/cm^2) and down to a minimal possible value for $\tau_{bulk,0}$ of 2 ms. This suggests a minimal influence of J_0 and $\tau_{bulk,0}$ components, and hence an accurate parameterization of the B-O related recombination properties. It should be noted that attempts to fit the data using a recent parameterization presented in [49], failed. In the early stages of degradation, a reasonable fit could only be obtained with a value of $\tau_{bulk,0}$ of 2.5 ms. However, this did not allow a reasonable fit at subsequent stages of degradation. To obtain such a fit throughout rapid degradation, the value of $\tau_{bulk,0}$, which should be time-independent, had to be reduced. Furthermore, $\tau_{bulk,0}$ was decreased to values well below the minimum allowed value of 1.8 ms, and hence the fits were meaningless.

A key difference between the parameterization presented in this work to that in [49] is the recombination properties of the acceptor level. In particular, for the parameterization presented in this work, the acceptor level of the defect has a much stronger influence in reducing carrier lifetime in high injection conditions. When simulating lifetime curves, if the assumed recombination caused by the acceptor level is too low and does not sufficiently describe the actual recombination from the acceptor level, then an appropriate reduction in the $\tau_{bulk,0}$ must be assumed, to effectively include a B-O related component. However, this $\tau_{bulk,0}$ value should remain unchanged throughout the degradation process. If a B-O related lifetime component for the acceptor level is inadvertently incorporated into this time-independent $\tau_{bulk,0}$ value, then an appropriate fit will not be obtained during subsequent (or possibly earlier) stages of degradation. High lifetime samples with low J_0 values, as are used in this work, will be most sensitive to this effect.

For the data presented in this work, we conclude that the acceptor level of the B-O defect has a stronger influence in reducing the τ_{eff} in high-injection than has been determined previously.

3. Modelling a multi-stage degradation of carrier lifetime with a single defect

Although a multi-stage degradation of carrier lifetime can obviously be described by the formation of two independent defects with different formation rates, it can also be described using a single defect. In our recent work, we presented a model to describe the multi-stage B-O related degradation with a single defect [1],[2]. In this model, assuming the existence of a latent (recombination inactive) B-O defect complex [40], there are two metastable recombination inactive configurations of the latent defect complex, corresponding to a *Stage 1 defect precursor* (S1DP) and a *Stage 2 defect precursor* (S2DP). Furthermore, there is an equilibrium between the populations in the S1DP and S2DP states, with thermally and/or carrier injection activated reactions to shift between the S1DP and S2DP states. We then assume that the S2DP is the direct

defect precursor state of the recombination active B-O defect and that the S1DP state is the precursor state of the S2DP state. Hence, the S1DP is the precursor of the *actual defect precursor*. If the defect formation rate (transition from the S2DP to the recombination active B-O complex) is significantly faster than the transition from S1DP to S2DP, then a multi-stage degradation of carrier lifetime will occur, as long as there is an initial non-zero population of both the S1DP and S2DP states. This model can be described by the following system of ordinary differential equations (ODEs) (Equations 1-3), where N_{S1DP}, N_{S2DP} and N_{BO} are the normalised concentrations of the S1DP, S2DP and the recombination active B-O defect complex states, respectively. Here, the reaction rate $\kappa_{S1DP \rightarrow S2DP}$ corresponds to the formation rate of the S2DP from the S1DP state, and the reaction rate $\kappa_{S2DP \rightarrow BO}$ corresponds to the B-O defect formation rate from the S2DP state. It should be noted that only forward reactions for the transition from S1DP to S2DP, and from S2DP to recombination active B-O complexes are considered. That is, the impact of dark annealing is not included in this system of ODEs, which is valid when investigating degradation at room temperature.

$$\frac{dN_{S1DP}}{dt} = -\kappa_{S1DP \rightarrow S2DP} \cdot N_{S1DP} \quad (1)$$

$$\frac{dN_{S2DP}}{dt} = \kappa_{S1DP \rightarrow S2DP} \cdot N_{S1DP} - \kappa_{S2DP \rightarrow BO} \cdot N_{S2DP} \quad (2)$$

$$\frac{dN_{BO}}{dt} = \kappa_{S2DP \rightarrow BO} \cdot N_{S2DP} \quad (3)$$

This system of ODEs can then be used to describe the effective minority carrier lifetime at a given injection level during multi-stage B-O related degradation (see Reference [1] for further details).

4. Impact of interstitial iron on recombination properties

One argument for the existence of two separate defects being responsible for B-O related degradation in the fast and slow timescales was the determination of k values in the vicinity of 100 throughout early stages of degradation. In our previous paper [1], we suggested that the higher k value for the fast decay in earlier studies might have been influenced by the dissociation of iron-boron pairs, given the known behaviour and recombination activity of interstitial iron (Fe_i) and iron-boron (Fe_i-B) pairs [54]. Here we present theoretical and experimental evidence highlighting the potential impact of iron on B-O related degradation studies.

A numerical simulation was performed to determine an effective capture cross-section ratio of SRH recombination in the presence of B-O and Fe_i. We used the known recombination properties of Fe_i, k_{Fei}=286 [55], and the parameterisation for B-O defects from **Table 2**. For simplicity, all Fe_i in the Cz wafer was assumed as fully dissociated from boron. The typical *NDD* values after degradation in the fast timescale and after full degradation were estimated using measurements from lifetime test structures. The effective capture cross-section ratio was estimated by taking the ratio of the SRH lifetime at two injection levels, $\Delta n=10^{17}$ /cm^3 and $\Delta n=10^{12}$ /cm^3. Hereafter, this will be denoted as τ_{ratio}.

The simulated impact of Fe_i on the τ_{ratio} throughout B-O related degradation is shown in Figure 2. In the absence of Fe_i, the SRH lifetime is described by B-O related recombination properties with a constant τ_{ratio} ($\tau_{ratio,BO}$) throughout degradation of 7.4. This is substantially lower than the k value of the B-O defect donor level (k_d=18) due to the influence of the acceptor level in reducing the lifetime at high injection levels. The corresponding value for Fe_i related recombination in the absence of B-O related recombination ($\tau_{ratio,Fei}$) is 306. For a relatively small [Fe_i] of 1×10^{10} /cm^3, τ_{ratio} values of 21.2 and 8.9 were simulated for *NDD* values typical after fast and complete (slow) degradation, respectively. Increasing [Fe_i] leads to an increased τ_{ratio} for a given *NDD*. For [Fe_i] = 1×10^{11} /cm^3, respective τ_{ratio} values of 107 and 21.5 were obtained. Increasing the *NDD* for a given [Fe_i] decreases τ_{ratio}, resulting in a reducing τ_{ratio} value. This feature can potentially describe a higher apparent capture cross-section ratio during early stages of B-O related degradation. It also highlights the potential influence in modulating the recombination properties when fully degraded.

Gettering processes are often used in B-O defect studies to reduce the impact of iron [46],[56]. However performing a gettering step alone may not be sufficient to ensure that a sample is iron-free. For example, during subsequent thermal processing such as emitter diffusion, thermal oxidation or even fast-firing [57] for activation of surface passivation layers, iron can be released from precipitate sites and result in [Fe_i] approaching 1×10^{10} /cm^3 [58]. As demonstrated in Figure 2, such concentrations are sufficient to cause a substantial modulation of the recombination properties.

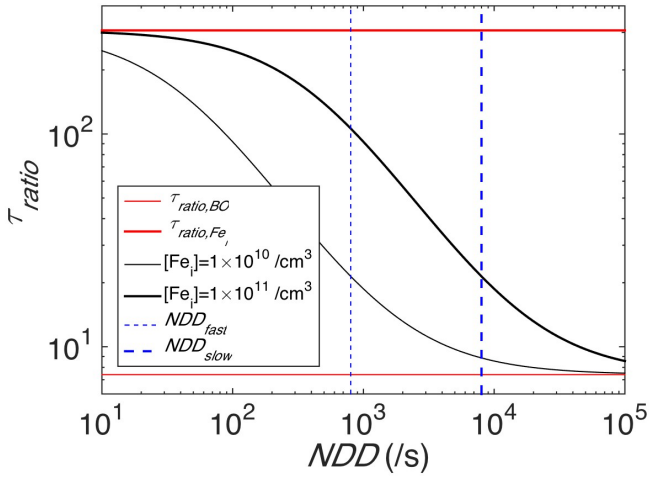

Figure 2 Ratio of SRH related lifetime in high injection ($\Delta n=10^{17}$ /cm^3), to low injection ($\Delta n=10^{12}$ /cm^3), τ_{ratio}, in the presence of interstitial iron (Fe_i) and B-O defects, for different concentrations of Fe_i (1×10^{10} /cm^3 or 1×10^{11} /cm^3)

as a function of the normalised defect density (*NDD*) for B-O related degradation. Dashed lines indicate typical *NDD* values after degradation in the fast timescale (NDD_{fast}) and after full degradation in the slow timescale (NDD_{slow}). Red solid lines represent the *k* value of B-O related recombination with no iron ($\tau_{ratio,BO}$) and Fe_i related recombination with no B-O defects ($\tau_{ratio,Fei}$).

If using subtraction techniques to determine the difference between two lifetime curves [11], a further complication can occur for studying B-O related degradation. In this instance, the dissociation of Fe_i-B pairs and therefore activation of Fe_i causes an increase in the iron-related SRH lifetime component at injection levels higher than the crossover point ($\Delta n > 10^{14}$ /cm^3) [54]. This results in a shrinking the difference between the curves in high injection and subsequent increase in the apparent τ_{ratio} value, leading to the determination of higher apparent capture cross section ratios.

To experimentally demonstrate this influence of Fe_i, symmetrical lifetime test structures were fabricated on *p*-type Cz 156 mm × 156 mm wafers with a resistivity of 1.6 Ω.cm that have a background [Fe_i] of approximately 3×10^{11} /cm^3. Samples were $POCl_3$ diffused to a sheet resistance of approximately (60 Ω/□) resulting in [Fe_i]~8×10^{10} /cm^3. Hydrogenated silicon nitride (SiN_x:H) with a refractive index of 2.08 was deposited on both sides of the samples using PECVD [59] in a Roth & Rau MAiA system. Lifetime measurements were performed after a conventional 200 °C dark anneal for 10 min and resting in the dark overnight to relax Fe_i back into Fe_i-B pairs, as well as after full degradation (48 hours illumination at 25 °C) and again allowing the iron to rest back into Fe_i-B pairs. Measurements were also taken at various stages after the activation of Fe_i on the fully degraded sample. Lifetime measurements were performed using a WCT-120 QSS-PC tool [60]. The measured data was analysed using generalised method [51] and corrected for Auger recombination [61]. For detecting the concentration of the presence of iron, the difference in lifetimes before and after short periods of illumination was used to identify the iron concentration, at a carrier concentration of $\Delta n = 9.1 \times 10^{14}$ /cm^3 ($0.1\times N_A$) [54].

The impact of Fe_i is shown in Figure 3. A subtraction of inverse effective minority lifetime curves between the fully degraded ($1/\tau_{eff,DG}$) and dark annealed ($1/\tau_{eff,DA}$) states was used to estimated the inverse SRH related lifetime ($1/\tau_{SRH}$) throughout B-O related degradation. For the dark annealed state, no activation of Fe_i was performed. In the light-soaked state, a comparison between curves with and without activation of the Fe_i is shown. Therefore, the curve without activation of Fe_i (black circles) more closely represents B-O related degradation, whereas the curve with activation of Fe_i (red circles) represents B-O related degradation including the influence of Fe_i. As shown, data without activation of Fe_i resulted in an expected low ratio of the SRH related lifetime in high and low injections (a ratio of 6.5 between $\Delta n = 7\times10^{15}$ /cm^3 and $\Delta n = 1\times10^{14}$ /cm^3. In contrast, comparing a sample with activation of Fe_i in the light-soaked state caused a substantial increase in this ratio (~230), evident by the much lower $1/\tau_{SRH}$ value in high injection, approaching zero for $\Delta n \sim 1\times10^{16}$ /cm^3. This demonstrates the significant potential modulation of the apparent capture cross-section ratios in the presence of iron.

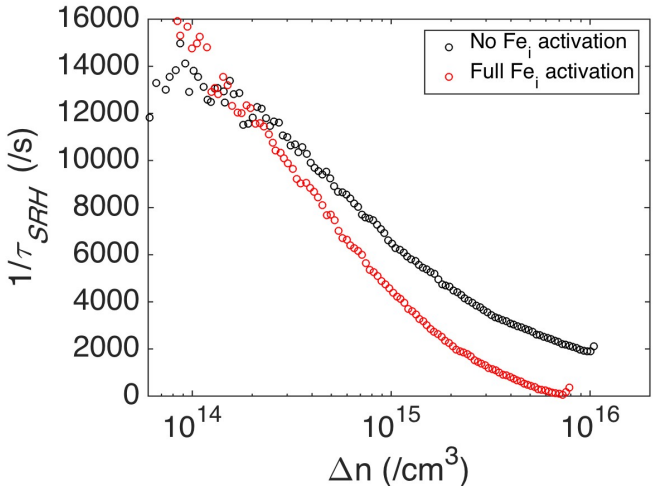

Figure 3 Inverse SRH related lifetime from a subtraction of injection-level-dependent inverse effective lifetime curves between the light-soaked ($1/\tau_{eff,DG}$) and dark annealed ($1/\tau_{eff,DA}$) states, with and without activation of interstitial iron (Fe_i) in the light-soaked state.

A recent contribution also suggested that only recombination from the 'SRC' could be passivated during permanent deactivation processes and that recombination activity associated with the 'FRC' remained [4]. To investigate the recombination properties of the samples after permanent deactivation, additional symmetrical lifetime structures as detailed above. In this instance, samples were phosphorus pre-gettered using a $POCl_3$ diffusion with a sheet resistance of 40 Ω/□, followed by the removal of the diffusion in an alkaline texturing solution. After the subsequent phosphorus diffusion (60 Ω/□), a low temperature anneal was then applied at 650 °C for 12 hours in a nitrogen ambient to precipitate any interstitial iron not removed during the gettering step [62]. This resulted in undetectable concentrations of interstitial iron using a known method based on photoconductance decay [54]. 75 nm of SiN_x:H (refractive index of 2.08) was deposited on both sides of the wafers using PECVD. Samples were then fired with a peak temperature of 740 °C. The samples were then degraded at room temperature, with lifetime measurements taken after 1000 s of illumination at 30 °C (for fast degradation) and after 48 hours light-soaking (for slow degradation). Hydrogen passivation of the B-O defects was performed using an illuminated annealing process at 180 °C for 2 hours [29],[63]–[65].

Curves on Auger-corrected inverse effective minority carrier lifetime are shown in Figure 4 at various stages of processing. Curves are shown directly after the fast firing process (typical of samples in the dark-annealed

state) after 1000 s of illumination (fast degradation) and after 48 hours of illumination (slow degradation). A further curve is shown after the hydrogen passivation process and a subsequent stability check (48 hours light soaking at room temperature). As shown, identical recombination properties are observed directly after firing in an unstable lifetime state, to the stable hydrogen passivated state. This demonstrates that both recombination occurring in the fast and slow timescales can be permanently avoided through the hydrogen passivation process. However, in iron-containing samples, the concentration of [Fe_i] was not significantly modulated during the permanent passivation process, resulting in the potential of recombination with a high-capture cross section ratio remaining after the permanent passivation process when the interstitial iron is activated (not shown). Hence the results presented in this paper with Fe_i can explain several features reported in the literature in B-O related studies.

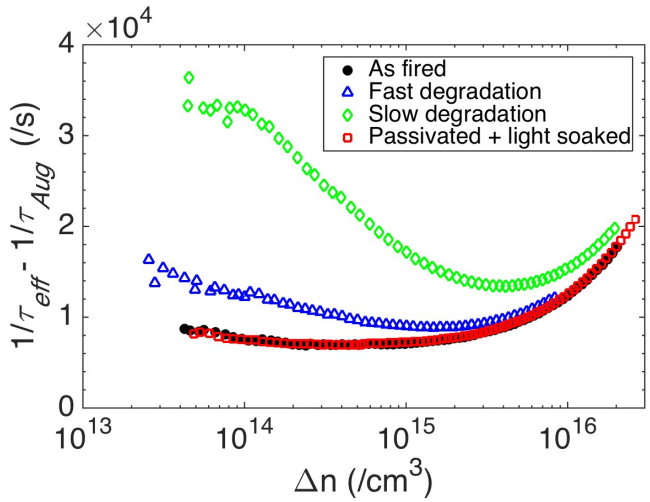

Figure 4 Curves of Auger-corrected inverse effective minority carrier lifetime after fast-firing (As fired), after 1000 seconds of illumination (fast degradation), after 48 hours of illumination (slow degradation), and after a 2 hour illuminated annealing process at 180 °C and subsequent 48 hour light soak (passivated + light soaked).

5. Modulating the extent of fast and slow B-O related degradation

In our earlier work, preliminary data demonstrated that changing the duration of dark annealing at 200 °C on pre-degraded samples could modulate the normalised defect density of samples within first 1000 seconds of subsequent illumination [1]. Our subsequent work demonstrated the ability to modulate the extent of fast and slow B-O related degradation using thermal annealing [2].

To demonstrate the modulation of fast and slow degradation by thermal annealing, symmetrical lifetime test structures were fabricated in accordance with the pre-gettered samples in Section 4. However, to suppress any permanent passivation of B-O defects during the illuminated processes, the samples were left non-fired [66]. Samples were initially annealed at 200 °C for 10 min on a hotplate to obtain the lifetime of the samples when B-O defects are completely annihilated, $\tau_{eff,DA}$. A metal plate with a vacuum was used to ensure good thermal contact to the hotplate and adequate temperature control. Throughout dark annealing, the temperature was monitored using a contact thermocouple, resulting in temperature fluctuations within ±1 °C. Subsequently, the samples were light soaked for 48 hours under 0.2 Suns illumination at approximately 35 °C to form all B-O defects, and obtain the lifetime of the samples in the fully degraded state, $\tau_{eff,DG}$ [8]. Further processing details can be seen in [2].

After full degradation, the samples were annealed at various temperatures for various times (Table 3) to investigate the impact of the annealing on the B-O related degradation. Subsequently, light soaking was performed at room temperature with *in-situ* lifetime measurements. All wafers were characterised using a Sinton Instruments WCT-120 quasi-steady-state photo-conductance QSS-PC tool [60] and analysed using the generalised technique [51]. *In-situ* lifetime measurements were recorded throughout the degradation process with a bias light (0.02 suns intensity) [8], which remained on during the in-situ measurements. The lifetime curves were corrected for the bias light. For all lifetime measurements, an excess carrier concentration of $\Delta n = 0.1 \cdot N_a$ was used.

Table 3 dark annealing time and temperature conditions

T (°C)	Time (sec)
155	25200
173	60
200	50, 100, 600

From the effective minority carrier lifetime measurements, the normalised defect density, $NDD(t)$, was determined using the following equation [67]:

$$NDD(t) = \frac{1}{\tau_{eff,LS}(t)} - \frac{1}{\tau_{eff,DA}} \quad (7)$$

Where $\tau_{eff,LS}(t)$ is the effective minority carrier lifetime after t seconds of light soaking. From Equation 7 above, the saturated normalised defect density (after full degradation), NDD_{DG} can be defined by:

$$NDD_{DG} = \frac{1}{\tau_{eff,DG}} - \frac{1}{\tau_{eff,DA}} \quad (8)$$

Where $\tau_{eff,DG}$ is the effective lifetime after full degradation. Using $NDD(t)$ and NDD_{DG}, fractional defect densities (FDD), which represent the percentages of B-O defects that were formed respectively to the total amount of defects after full degradation, were calculated using the following:

$$FDD = \frac{NDD(t)}{NDD_{DG}} \quad (9)$$

The thermal annealing performed on pre-degraded samples greatly impacted the subsequent degradation behaviour of the samples. Figure 5 shows the *FDD* throughout degradation after various dark anneals. Depending on the conditions used, a subsequent degradation under illumination could occur with almost all degradation occurring in the fast or slow timescales, or anywhere in between. For example, using a dark-annealing condition of 200 °C for 50 s was sufficient to annihilate all B-O defects, but cause approximately 70% of subsequent degradation to occur in the fast timescale. Increasing the annealing time at 200 °C decreased the extent of degradation occurring in the fast timescale, down to approximately 15% for an annealing duration of 600 s. Using an annealing temperature of 155 °C for 7 hours resulted in a further reduction in the extent of rapid degradation. It should be noted that the *NDD* at full degradation was in the range of 6.9×10^{-3} – 7.9×10^{-3} /s for all samples. The small differences in *NDD* may have been caused by thermally related effects leading to a permanent reduction in the concentration of S1DP, similarly to what can occur with high-temperature processing [4].

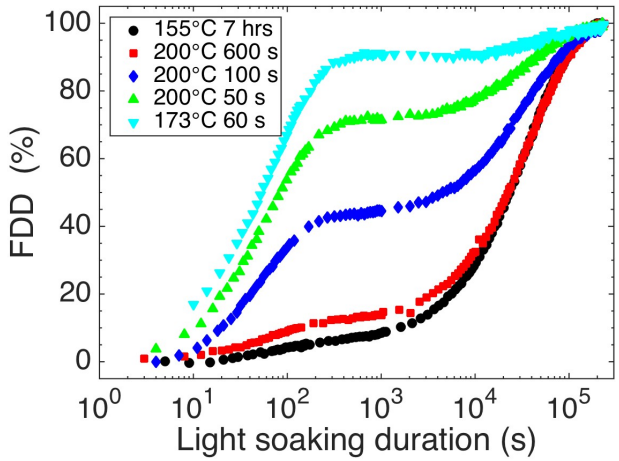

Figure 5 *FDD* determined from in-situ lifetime measurements of after various dark annealing conditions. The dotted lines are fitted with two exponential decay curves. Data from [2].

Further investigations in [2] determined an activation of E_a = 0.91 ± 0.10 eV and attempt frequency of ν = 2×10^{8} /s for the reduction in *FDD* that occurs in the fast timescale. This confirmed that an additional reaction occurs during dark annealing, beyond simply removing the recombination activity of the B-O defects. That paper also demonstrated identical recombination properties of degradation in the fast and slow timescales on samples deliberately manipulated to cause almost all degradation to occur in the respective timescales [2]. The results suggest a vital link between the defect that is responsible for both the fast and slow B-O related degradation. Furthermore, this is not consistent with published defect theories that suggest the involvement of two separate defects and a formation mechanism based on the reconfiguration of latent based B-O complexes (i.e. a non-diffusion-based mechanism for defect formation) [4]. Hence, the ability to modulate the extent of fast and slow degradation provides further evidence for the involvement of a single defect.

6. A revised defect model

All experimental results in the former sections of this paper strongly suggest the involvement of a single B-O defect being responsible for both the fast and slow degradation of minority carrier lifetime. The identical recombination properties observed throughout degradation indicates that either, only a single defect is responsible for both the fast and slow degradation of carrier lifetime, or that if two different defects are involved, any difference in recombination properties between the defects is negligible. The identification of indistinguishable recombination properties takes away one key argument for the existence of two separate defects. Kinetic modelling is also able to adequately describe a multi-stage degradation of carrier lifetime using a single recombination active defect. Evidence was presented of a possible involvement of interstitial iron in modulating the injection level dependent lifetime curves, particularly during early stages of B-O degradation, and could also explain a recent observation of recombination with a high capture cross section ratio (normally attributed to the FRC), remaining after a permanent deactivation process. Furthermore, dark annealing was observed to modulate the fraction of fast and slow degradation, without modulating the total extent of degradation or recombination properties [2]. The determination of an activation energy and attempt frequency for the reduction in the extent of degradation in the fast timescale after dark annealing provides a vital link between degradation in the two timescales, again pointing towards the involvement of a single defect.

On the basis of this new evidence, we present a revised defect formation model. This understanding is independent of whether the defect formation mechanism is due to a diffusion-based or a latent-based mechanism. We describe the system for defect formation with three states (see Figure 6). States A1 (the *Stage 1 defect precursor*) and A2 (the *Stage 2 defect precursor*) are recombination inactive and are equivalent to State A in a conventional three-state model describing the permanent deactivation of B-O defects [29]. State B is the recombination active defect state.

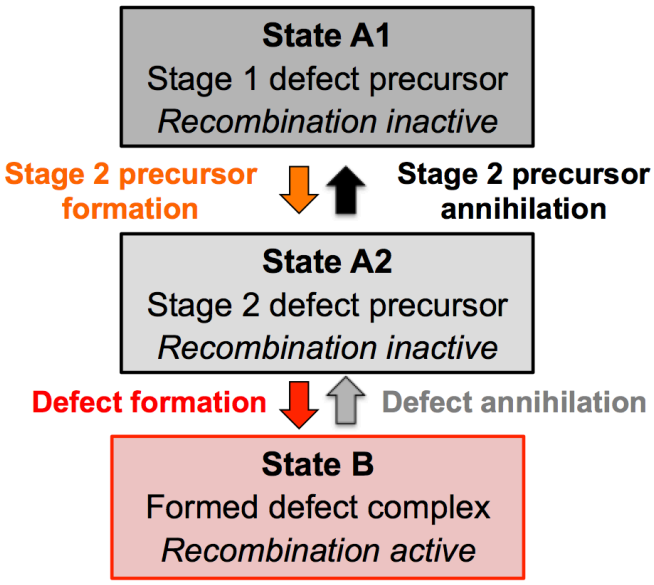

Figure 6 Diagram of the model for B-O defect formation.

The transition from state A1 to state A2 is related to the formation of the *Stage 2 defect precursor* from the *Stage 1 defect precursor*. That is, the transition does not directly cause degradation of the silicon as no recombination active defects are formed during this reaction. This transition occurs in the slow timescale that is normally attributed to the SRC. This transition is driven both by the availability of electrons and holes, and hence carrier-enhanced [8], with a quadratic dependence on holes [68]. In the literature, this reaction has an activation energy of 0.475 ± 0.035 eV and attempt frequency of 4×10^{3} /s for p-type silicon with a boron doping concentration of $1x10^{16}$ /cm^{3} [11].

The transition from state A2 to state B is related to the recombination-active defect formation from the *Stage 2 defect precursor*. This reaction is responsible for the degradation of carrier lifetime. This is a relatively rapid reaction, with a time-scale approximately two orders of magnitude higher than that of the transition from state A1 to state A2 at room temperature, corresponding to the fast time-scale of degradation normally attributed to the FRC. This reaction is also carrier-carrier-enhanced, again with a dependence on the availability of electrons and quadratic dependence on holes [49]. In the literature, this reaction has an activation energy of 0.23±0.02 eV and attempt frequency of 125 /s for p-type silicon with a boron doping concentration of 1.4 Ω·cm [24].

In this model, the slow reaction (transition from state A1 to state A2) is a *precursor reaction* of the faster reaction for defect formation (from state A2 to state B). The origin of the multi-stage degradation during light soaking comes from the silicon material possessing non-zero populations in both states A1 and A2 after a specific thermal process. Any population starting in state A2 (*Stage 2 defect precursors*) can proceed to defect formation immediately. This is responsible for the fast time-scale of degradation (normally attributed to the FRC). On the other hand, any population starting in A1 is not immediately available for defect formation, but must first undergo the slow transition into state A2 (*Stage 2 defect precursor*s), before the more rapid defect formation reaction can take place. As a result, the initial population in state A1 is responsible for the slow degradation (normally attributed to the SRC). Thermal processing can modulate the populations in states A1 and A2. This is particularly evident when performing dark annealing on pre-degraded samples.

The transition from state B to state A2 represents the annihilation of the B-O defects, and hence the recovery of carrier lifetime during dark annealing. This recovery of minority carrier lifetime is not stable, and the samples will again degrade under subsequent illumination. The literature value for this reaction has an activation energy of 1.32 ± 0.05 eV and attempt frequency of 1×10^{13} /s [11].

The transition from state A2 to A1 occurs with prolonged dark annealing. This represents the annihilation of the *Stage 2 defect precursor* into another recombination inactive species, the *Stage 1 defect precursor*. The literature value for this reaction has an activation energy of 0.91 ± 0.10 eV with a corresponding attempt frequency of 2×10^{8} /s.

7. Summary

B-O related degradation has often been attributed to two separate defects for the degradation that occurs in the fast and slow timescales. The arguments include differing capture cross-section ratios determined in early studies [11], different time constants of degradation [10] and recombination activity associated with degradation in the fast timescale remaining after permanent deactivation processes [4]. However new evidence has emerged to suggest that B-O related degradation could be caused by a single defect. Key arguments for the involvement of a single defect are:

1) The ability to describe the two-stage degradation in carrier lifetime by a single set of recombination properties all throughout the degradation process [1]. In particular, a capture cross-section ratio of $\sigma_{n,d}/\sigma_{p,d} = 18$ was determined for the donor level of the defect. This value is substantially lower than earlier determinations for the capture cross-section ratio of degradation in the fast time scale in the range of 65-100.

2) A multi-stage degradation of carrier lifetime was theoretically simulated using kinetic modelling using a single recombination active defect [1]. For this, two recombination inactive states exist, namely *Stage 1 defect precursors* and *Stage 2 defect precursors*. A multi-stage degradation can occur when there is a non-zero population in both defect precursor states, and a slow reaction rate exists for the transformation of S1DP into the S2DP state. Subsequently, there is a more rapid reaction of defect formation, as the transformation from the S2DP state into the recombination active B-O defect.

3) The presence of interstitial iron, even in very small concentrations can significantly affect the

recombination properties when studying B-O related degradation. Fe_i can cause higher apparent capture cross-section ratios, particularly during early stages of degradation. Furthermore, we show that all B-O related degradation in either the fast or slow timescales can be passivated during illuminated annealing. However, the processes do not effectively passivate Fe_i, leaving the potential for the recombination properties of Fe_i to remain after permanent deactivation of the B-O defect.

4) Thermal annealing performed on pre-degraded samples can modulate the fraction of degradation during subsequent annealing that occurs in the fast and slow timescales [2]. This suggests a vital link between the two recombination-inactive states that is not consistent with current theories suggesting the involvement of two separate defects. Furthermore, this modulation occurs with no change in recombination properties, providing further evidence of a single defect.

Finally, a revised defect model is presented with a single B-O defect. Here, two recombination inactive states exist in the silicon, with a third recombination active state. The multi-stage degradation occurs due to an initial mix of the two recombination-inactive states. Any initial population in the *Stage 2 defect precursor* state, A2, can rapidly form defects. The other recombination inactive state is the precursor of the *Stage 2 defect precursor*, namely the *Stage 1 defect precursor*, state A1. Hence any population in state A1 must undergo a slow transition into the state A2, before the more rapid defect formation reaction takes place.

Acknowledgements

The authors would like to acknowledge Daniel Chen, Kyung Kim, Ly Mai, Hongzhao Li, and the MAiA processing team who assisted with wafer processing. This Program has been supported by the Australian Government through the Australian Renewable Energy Agency (ARENA) and the Australian Center for Advanced Photovoltaics (ACAP). The views expressed herein are not necessarily the views of the Australian Government, and the Australian Government does not accept responsibility for any information or advice contained herein. T. U. Nærland acknowledges funding from "The Norwegian Research Centre for Solar Cell Technology" and REC Wafer, REC Solar, Elkem Solar and the Norwegian Research Council through the KMB project "Defect engineering for crystalline silicon solar cells". The authors would like to thank the commercial partners of the ARENA 1-A060 project, and the UK Institution of Engineering and Technology (IET) for their funding support for this work through the A.F. Harvey Engineering Prize.

References

[1] B. Hallam, M. Abbott, T. Nærland, and S. Wenham, Phys. Status Solidi (RRL)-Rapid Res. Lett. **10**, 520 (2016).

[2] M. Kim, M. Abbott, N. Nampalli, S. Wenham, B. Stefani, and B. Hallam, J. Appl. Phys. **121**, 53106 (2017).

[3] H. Fischer and W. Pschunder., in *Proc. 10th IEEE Photovolt. Spec. Conf.* (IEEE, 1973), pp. 404–411.

[4] V. Voronkov and R. Falster, Phys. Status Solidi **253**, 1721 (2016).

[5] D.C. Walter, B. Lim, K. Bothe, V. V Voronkov, R. Falster, and J. Schmidt, Appl. Phys. Lett. **104**, 42111 (2014).

[6] N. Nampalli, B.J. Hallam, C.E. Chan, M.D. Abbott, and S.R. Wenham, Photovoltaics, IEEE J. **5**, 1580 (2015).

[7] C. Möller and K. Lauer, Phys. Status Solidi (RRL)-Rapid Res. Lett. **7**, 461 (2013).

[8] J. Schmidt and K. Bothe, Phys. Rev. B **69**, 24107 (2004).

[9] J. Knobloch, S.W. Glunz, V. Henninger, W. Warta, W. Wettling, F. Schomann, W. Schmidt, A. Endros, K. Münzer, A. Endrös, and K.A. Münzer., in *Proc. 13th Eur. Photovolt. Sol. Energy Conf.* (1995), pp. 9–12.

[10] H. Hashigami, M. Dhamrin, and T. Saitoh, Japanese J. Appl. Physics, Part 1 Regul. Pap. Short Notes Rev. Pap. **42**, 2564 (2003).

[11] K. Bothe and J. Schmidt, J. Appl. Phys. **99**, 13701 (2006).

[12] K. Bothe, J. Schmidt, and R. Hezel, Photovolt. Energy Conversion, 2003. Proc. 3rd World Conf. **2**, 1077 (2003).

[13] T.U. Nærland, H. Haug, H. Angelskar, R. Sondena, E.S. Marstein, and L. Arnberg, Photovoltaics, IEEE J. **3**, 1265 (2013).

[14] T. Niewelt, J. Sch, W. Warta, S.W. Glunz, and M.C. Schubert, IEEE J. Photovoltaics **7**, 383 (2017).

[15] M. Forster, E. Fourmond, F.E. Rougieux, A. Cuevas, R. Gotoh, K. Fujiwara, S. Uda, and M. Lemiti, Appl. Phys. Lett. **100**, 42110 (2012).

[16] J. Knobloch, S.W.W. Glunz, D. Biro, W. Warta, E. Schaffer, and W. Wettling, in *Proc. 25th IEEE Photovolt. Spec. Conf.* (1996), pp. 405–408.

[17] J. Schmidt, A.G. Aberle, and R. Hezel, in *Proc. 26th IEEE Photovolt. Spec. Conf.* (1997), pp. 13–18.

[18] B. Lim, K. Bothe, and J. Schmidt, Phys. Status Solidi - Rapid Res. Lett. **95**, 93 (2008).

[19] J. Schmidt, K. Bothe, and R. Hezel, in *Conf. Rec. Twenty-Ninth IEEE Photovolt. Spec. Conf. 2002.* (2002), pp. 178–181.

[20] B. Lim, F. Rougieux, D. Macdonald, K. Bothe, and J. Schmidt, J. Appl. Phys. **108**, 103722 (2010).

[21] T. Schutz-Kuchly, J. Veirman, S. Dubois, and D.R. Heslinga, Appl. Phys. Lett. **96**, 93505 (2010).

[22] S.M. Kim, S. Chun, S. Bae, S. Park, M.G. Kang, H. Song, Y. Kang, H. Lee, and D. Kim, Appl. Phys. Lett. **105**, 83509 (2014).

[23] S. Rein, T. Rehrl, W. Warta, S.W. Glunz, and G. Willeke, Proc. 17th Eur. Photovolt. Sol. Energy Conf. 1555 (2002).

[24] K. Bothe and J. Schmidt, Appl. Phys. Lett. **87**, 262108 (2005).

[25] K. Bothe, R. Hezel, and J. Schmidt, Appl. Phys.

Lett. **83**, 1125 (2003).
[26] D.W. Palmer, K. Bothe, and J. Schmidt, Phys. Rev. B **76**, 35210 (2007).
[27] K. Bothe, J. Schmidt, and R. Hezel, Proc. 29th IEEE Photovolt. Spec. Conf. 194 (2002).
[28] H. Hashigami, Y. Itakura, and T. Saitoh, J. Appl. Phys. **93**, 4240 (2003).
[29] A. Herguth, G. Schubert, M. Käs, and G. Hahn, Proc. 4th IEEE World Conf. Photovolt. Energy Convers. **1**, 940 (2006).
[30] S.Y. Lim, F.E. Rougieux, and D. Macdonald, Appl. Phys. Lett. **103**, 92105 (2013).
[31] T. Mchedlidze and J. Weber, Phys. Status Solidi (RRL)-Rapid Res. Lett. **9**, 108 (2015).
[32] M. Forster, P. Wagner, J. Degoulange, R. Einhaus, G. Galbiati, F.E. Rougieux, A. Cuevas, and E. Fourmond, Sol. Energy Mater. Sol. Cells **120**, 390 (2014).
[33] F.E. Rougieux, B. Lim, J. Schmidt, M. Forster, D. Macdonald, and A. Cuevas, J. Appl. Phys. **110**, 63708 (2011).
[34] A. Herguth, G. Schubert, M. Käs, and G. Hahn, Prog. Photovoltaics Res. Appl. **16**, 135 (2008).
[35] T.U. Nærland, H. Angelskår, and E.S. Marstein, J. Appl. Phys. **113**, 193707 (2013).
[36] L.I. Khirunenko, Y. V Pomozov, M.G. Sosnin, and A. V Duvanskii, Solid State Phenom. **178–179**, 178 (2011).
[37] J. Schmidt and A. Cuevas, J. Appl. Phys. **86**, 3175 (1999).
[38] G. Krugel, W. Wolke, J. Geilker, S. Rein, and R. Preu, Energy Procedia **8**, 47 (2011).
[39] J.H. Reiss, R.R. King, and K.W. Mitchell, Appl. Phys. Lett. **68**, 3302 (1996).
[40] V. V Voronkov and R. Falster, J. Appl. Phys. **107**, 53509 (2010).
[41] S. Rein and S.W. Glunz, Appl. Phys. Lett. **82**, 1054 (2003).
[42] F.E. Rougieux, M. Forster, D. Macdonald, A. Cuevas, B. Lim, and J. Schmidt, IEEE J. Photovoltaics **1**, 54 (2011).
[43] V. V Voronkov and R. Falster, Solid State Phenom. **205–206**, 3 (2014).
[44] V. V Voronkov, R. Falster, K. Bothe, B. Lim, and J. Schmidt, J. Appl. Phys. **110**, 63515 (2011).
[45] N. Nampalli, T.H. Fung, S. Wenham, B. Hallam, M. Abbott, and M. Abbott, Front. Energy **11**, 4 (2017).
[46] T. Niewelt, J. Schön, J. Broisch, W. Warta, and M. Schubert, Phys. Status Solidi (RRL)-Rapid Res. Lett. **9**, 692 (2015).
[47] V. V Voronkov, R.J. Falster, B. Lim, and J. Schmidt, ECS Trans. **50**, 123 (2013).
[48] V. V Voronkov, R. Falster, and A. V Batunina, Phys. Status Solidi **208**, 576 (2011).
[49] T. Niewelt, S. Mägdefessel, and M.C. Schubert, J. Appl. Phys. **120**, 85705 (2016).
[50] R.A. Sinton, A. Cuevas, and M. Stuckings, in *Proc. 25th IEEE Photovolt. Spec. Conf.* (1996), pp. 457–460.
[51] H. Nagel, C. Berge, and A.G. Aberle, J. Appl. Phys. **86**, 6218 (1999).
[52] A. Cuevas and D. Macdonald, Sol. Energy **76**, 255 (2004).
[53] W. Shockley and W.T. Read Jr, Phys. Rev. **87**, 835 (1952).
[54] D.H. Macdonald, L.J. Geerligs, and A. Azzizi, J. Appl. Phys. **95**, 1021 (2004).
[55] D. MacDonald, T. Roth, P.N.K. Deenapanray, T. Trupke, and R.A. Bardos, Appl. Phys. Lett. **89**, 142107 (2006).
[56] S. Wilking, M. Forster, A. Herguth, and G. Hahn, Sol. Energy Mater. Sol. Cells **142**, 87 (2015).
[57] D. Macdonald, A. Cheung, and A. Cuevas, in *3rd World Conf. onPhotovoltaic Energy Conversion, 2003. Proc.* (2003), pp. 11–14.
[58] B. Hallam, D. Chen, M. Kim, B. Stefani, B. Hoex, M. Abbott, and S. Wenham, Submitt. to Phys. Status Solidi A **1**, 1 (2017).
[59] Z. Hameiri, N. Borojevic, L. Mai, N. Nandakumar, K. Kim, and S. Winderbaum, in *43rd IEEE Photovolt. Spec. Conf.* (2016), pp. 2900–2904.
[60] R.A. Sinton and A. Cuevas, Appl. Phys. Lett. **69**, 2510 (1996).
[61] A. Richter, F. Werner, A. Cuevas, J. Schmidt, and S.W. Glunz, Energy Procedia **27**, 88 (2012).
[62] A.Y. Liu and D. Macdonald, J. Appl. Phys. **115**, 114901 (2014).
[63] B. Hallam, S. Wenham, P. Hamer, M. Abbott, A. Sugianto, C. Chan, A. Wenham, M. Eadie, and G. Xu, Energy Procedia **38**, 561 (2013).
[64] S. Wilking, A. Herguth, and G. Hahn, J. Appl. Phys. **113**, 194503 (2013).
[65] K. Münzer, in *Proc. 24th Eur. Photovolt. Sol. Energy Conf. Hambg.* (2009), pp. 1558–1561.
[66] B.J. Hallam, S.R. Wenham, P.G. Hamer, M.D. Abbott, A. Sugianto, C.E. Chan, A.M. Wenham, M.G. Eadie, and G. Xu, Energy Procedia **38**, 561 (2013).
[67] S.W. Glunz, S. Rein, W. Warta, J. Knobloch, and W. Wettling, Sol. Energy Mater. Sol. Cells **65**, 219 (2001).
[68] P. Hamer, N. Nampalli, Hameiri Ziv, M. Kim, D. Chen, N. Gorman, B. Hallam, M. Abbott, and S. Wenham, Energy Procedia **92**, 791 (2016).